https://doi.org/10.21122/2227-1031-2026-25-1-32-41

UDC 621.923.7

Effect of Electrolyte-Plasma Treatment on the Structure and Surface Properties of Medical-Grade Corrosion-Resistant Steels

A. Yu. Korolyov[1)], V. A. Tomilo[1)], V. S. Niss[1)], S. V. Grigoriev[1)]

[1)]Belarusian National Technical University (Minsk, Republic of Belarus)

Abstract. This paper presents the results of a study on the effect of Electrolytic-Plasma Treatment (EPT) parameters on the structure and properties of the surface layer of austenitic corrosion-resistant steels AISI 304, AISI 316L, and AISI 321, which are widely used in the production of medical devices. As a result of EPT, inhomogeneities in the form of chromium carbide inclusions appear on the surface of AISI 304 steel samples; their size and quantity decrease with increasing treatment duration and become almost negligible after 10 min. For AISI 321 and AISI 316L steels, EPT primarily leads to surface smoothing through the removal of micro-irregularities without significant structural changes, while small, uniformly distributed titanium carbide particles up to 4 μm in size remain on the AISI 321 steel. The identified features of surface structure formation significantly affect the roughness: its most intensive change is observed at an EPT duration of 3–5 min, after which the dynamics decrease. Due to the relief formed by carbide inclusions, the roughness values of AISI 304 steel samples are higher than those of AISI 316 and AISI 321 steel samples. At voltages of 260–320 V, the roughness parameters remain stable; however, at 340 V, a deterioration in surface quality is observed due to the transition to an electrolytic-discharge mode. With an increase in EPT duration, the corrosion potential of all the studied corrosion-resistant steels shifts to the positive region, and the corrosion current density decreases by 6–7 times. The greatest improvements are observed for AISI 316L steel – the corrosion potential increases from ~184 to ~98 mV. The wetting contact angle increases sharply from ~58° to ~84° after 1–3 min of treatment, then stabilizes in the range of 85–88°, indicating an increase in surface hydrophobicity.

Keywords: electrolytic-plasma treatment, corrosion-resistant steel, structure, roughness, corrosion resistance, wetting contact angle

For citation: Korolyov A. Yu., Tomilo V. A., Niss V. S., Grigoriev S. V. (2026) Effect of Electrolyte-Plasma Treatment on the Structure and Surface Properties of Medical-Grade Corrosion-Resistant Steels. *Science and Technique*. 25 (1), 32–41. https://doi.org/10.21122/2227-1031-2026-25-1-32-41

Влияние электролитно-плазменной обработки на структуру и свойства поверхностного слоя коррозионностойких сталей медицинского назначения

Канд. техн. наук, доц. А. Ю. Королёв[1)], докт. техн. наук, проф. В. А. Томило[1)], канд. техн. наук, доц. В. С. Нисс[1)], инж. С. В. Григорьев

[1)]Белорусский национальный технический университет (Минск, Республика Беларусь)

Реферат. В работе представлены результаты исследования влияния параметров электролитно-плазменной обработки (ЭПО) на структуру и свойства поверхностного слоя аустенитных коррозионностойких сталей AISI 304, AISI 316L и AISI 321, широко применяемых при производстве изделий медицинского назначения. В результате ЭПО на поверхности образцов из стали AISI 304 выделяются неоднородности в виде включений карбида хрома, размеры и количество которых уменьшаются с увеличением продолжительности обработки и практически не проявляются после 10 мин. Для сталей AISI 321 и AISI 316L ЭПО приводит преимущественно к сглаживанию поверхности за счет удаления микронеровностей без существенных изменений структуры. При этом на стали AISI 321 сохраняются мелкие равномерно распределенные частицы карбида титана размером до 4 мкм. Установленные особенности формирования структуры поверхности существенно влияют на шероховатость: ее наиболее интенсивное изменение наблюдается при продолжительности ЭПО 3–5 мин, после чего динамика снижается. Из-за наличия рельефа из карбидных включений значения шероховатости образцов из стали AISI 304 выше, чем образцов из сталей AISI 316 и AISI 321. При напряжениях 260–320 В параметры шероховатости остаются стабильными, однако при 340 В наблюдается

Адрес для переписки
Королёв Александр Юрьевич
Белорусский национальный технический университет
ул. Я. Коласа, 24,
220013, г. Минск, Республика Беларусь
Тел.: +375 17 374-25-98
korolyov@park.bntu.by

Address for correspondence
Korolyov Aleksandr Yu.
Belarusian National Technical University
24, Ya. Kolasa str.,
220013, Minsk, Republic of Belarus
Tel.: +375 17 374-25-98
korolyov@park.bntu.by

ухудшение качества поверхности вследствие перехода в электролитно-разрядный режим. С увеличением продолжительности ЭПО потенциал коррозии всех исследованных коррозионностойких сталей смещается в положительную область, а плотность тока коррозии уменьшается в 6–7 раз. При этом наибольшие улучшения наблюдаются для стали AISI 316L – потенциал коррозии повышается с ~184 до ~98 мВ. Краевой угол смачивания после 1–3 мин обработки резко возрастает с ~58° до ~84°, после чего стабилизируется в диапазоне 85–88°, что указывает на повышение гидрофобности поверхности.

Ключевые слова: электролитно-плазменная обработка, коррозионностойкая сталь, структура, шероховатость, коррозионная стойкость, краевой угол смачивания

Для цитирования: Влияние электролитно-плазменной обработки на структуру и свойства поверхностного слоя коррозионностойких сталей медицинского назначения / А. Ю. Королёв [и др.] // *Наука и техника.* 2026. Т. 25, № 1. С. 32–41. https://doi.org/10.21122/2227-1031-2026-25-1-32-41

Introduction

The condition of the surface layer of implantable medical devices characterized by its structure, roughness and the presence of micro- and macro-defects and foreign inclusions has a dominant influence on their corrosion resistance and biocompatibility [1]. Reducing the height of micro-irregularities, the density of defects, impurities, and foreign inclusions in the surface layer minimizes the likelihood of negative consequences of implantation associated with potential corrosion damage, reactogenicity and fatigue failure. The condition of the surface layer is especially critical for the functioning of high-responsibility devices such as cardiovascular implants, including stents, artificial heart valves, filter traps and occluders. The surface topography of these devices determines their propensity to adsorb proteins and to adhere platelets and leukocytes after implantation [2]. Reducing roughness increases the wetting contact angle, i.e. leads to the formation of a hydrophobic surface. Upon contact of an implant with blood platelet adhesion on a hydrophobic surface is inhibited which reduces the potential thrombogenic risk [2–6]. A smooth stent surface reduces platelet activation and aggregation, thereby decreasing the likelihood of thrombus formation and neointimal hyperplasia [7–9].

Currently, the primary metallic materials used in the production of implants are stainless steel, titanium and titanium alloys, cobalt-chromium alloys, and nickel-titanium alloys (nitinol). Tantalum, magnesium alloys, and precious metals (silver, gold, platinum, palladium) are used less frequently [10]. Among these the most commonly used materials for manufacturing medical devices are austenitic-class stainless steels, due to their relatively low cost and good manufacturability [11–13]. To improve the surface quality of medical devices mechanical methods are employed with tumbling and magnetic abrasive polishing being the most common as well as electrochemical methods including electrolyte-plasma treatment (EPT). The application of the EPT method not only reduces roughness but also modifies the surface of medical devices enhancing its protective properties [14–17]. Conducted studies have demonstrated the high efficiency of using this method in the production of medical devices [18, 19]. Based on EPT, a number of new high-performance processes have been developed and implemented in production, ensuring improved surface quality for devices made from a wide range of medical materials, including stainless steels, titanium and titanium alloys, cobalt-chromium, and nickel-titanium alloys [14, 20–25].

However, despite proven effectiveness, systematic data on the relationship between EPT parameters, the resulting surface layer structure, and the final complex of functional properties critical for medical application are currently lacking. In particular, the patterns of influence of EPT parameters on such interconnected characteristics as roughness, corrosion resistance, and wettability which determine the surface hydrophilicity/hydrophobicity and its ability to interact with biological fluids require in-depth study. The aim of the present work is to establish quantitative and qualitative patterns of the influence of key EPT parameters on the formation of the structure and the complex of properties of the surface layer of medical-grade stainless steels.

Materials and Methods

For the research, plates measuring 30×10×1 mm made of stainless steels AISI 304, AISI 316L and AISI 321 were used. These steels are widely employed in the production of medical devices. Their chemical composition is presented in Table 1.

Table 1

Composition of medical-grade austenitic corrosion-resistant steels [26, 27]

Steel	C	Si	Mn	P	Cr	Ni	N	Mo	Ti	S
316L	0.03	–	1.95	0.02	17.2	12.6	0.05	2.40		–
304	0.06	0.46	1.32	0.03	18.2	9.1	0.04	–		0.04
321	0.12	max 0.8	max 2.00	max 0.045	17–19	8–9.5		–	max 0.70	0.03

The surface of the samples was pre-treated with P400 grit sandpaper. The average value of the roughness parameter *Ra* was 0.262 μm. For treatment the samples, the most commonly used electrolyte in the practice of EPT for stainless steel products, based on ammonium sulfate, was employed. The electrolyte concentration was 4 % and its temperature varied in the range of 70–90 °C. EPT was carried out at a voltage of 260–340 V. The EPT duration was 1–10 min.

The mass of the samples before and after EPT was measured using an OHAUS Pioneer PA 214C analytical balance with a resolution of 0.1 mg. The metal removal Δm was calculated using the formula:

$$\Delta m = \frac{m_{init} - m_{fin}}{m_{init}} \cdot 100\ \%, \qquad (1)$$

where m_{init} is the mass of the sample before EPT, m_{fin} is the mass of the sample after EPT.

Surface roughness was measured using a MarSurf PS1 profilometer with a base length Lt = 5.6 mm (cut-off wavelength λc = 0.8 mm; total measurement length – 4 mm). The surface structure of the samples was studied using an Altami MET1 metallographic microscope and a VEGA II LMU scanning electron microscope.

To evaluate the corrosion resistance of the sample surfaces, potentiodynamic studies were performed using a PI-50-Pro potentiostat. The potentiodynamic studies involved recording polarization curves and determining based on the obtained data the corrosion potential E_{corr}, corrosion current density i_{corr}, and pitting potential E_{pitt}. A three-electrode electrochemical cell was used to obtain the polarization curves. The cell included the test sample as the working electrode and a measurement system consisting of an auxiliary platinum electrode (model EPV-1SR-100), a silver/silver chloride reference electrode (EVL-1M3.1-100) and an electrolyte. A 3 % NaCl solution in distilled water at 20 °C was used as the electrolyte. Measurements were conducted in the central area of the sample with an area of 0.64 cm². The remaining part of the sample was coated with an insulating layer to prevent its influence on the measurement results.

The pitting potential E_{pitt} was determined from the potentiodynamic curve as the potential corresponding to the onset of a sharp current increase. To determine the corrosion potential E_{corr} and corrosion current density i_{corr}, plots of the decimal logarithm of current density lg$i$ versus potential were constructed. The corrosion potential E_{corr} values were determined from the intersection of the anodic and cathodic branches of the obtained curves. The corrosion current density was determined based on the analysis of the cathodic branch of the polarization curve [28]. A segment on the cathodic branch where the dependence of lg$i$ on potential was linear (the region of pure activation polarization) was identified. This linear segment was located 50–150 mV more negative than the corrosion potential. The identified linear segment was extrapolated into the region of more positive potentials until it intersected the abscissa corresponding to the corrosion potential E_{corr}. The intersection point of the lines determined the value of lgi_{corr} from which the corrosion current i_{corr} was calculated.

To assess surface wettability the static sessile drop method with subsequent analysis of its digital image was used to measure the wetting contact angle (θ). For this a 3–5 μl droplet of distilled water was deposited vertically onto the sample surface using a dosing syringe. The droplet shape was recorded within 5 s after deposition to achieve a stable state. Photographs with parameters providing the necessary magnification and clarity of the droplet-surface boundary were taken from a side projection. The images were analyzed using the «Kompas» software. The wetting contact angle θ was taken as the average value of the left and right angles determined on symmetrical sections of the droplet (Fig. 1). The measurement error associated with image resolution and contour determination accuracy did not exceed ±1°.

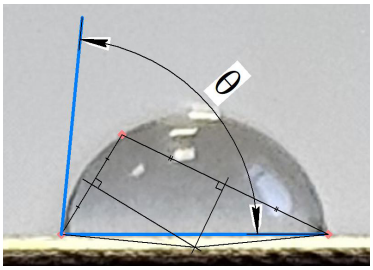

Fig. 1. Wetting contact angle measurement diagram

Results and Discussion

Fig. 2 presents micrographs of the surface of AISI 304 steel samples after EPT with durations of 1, 3, 5, 7.5, and 10 min at a voltage of 300 V in an electrolyte with a temperature of 90 °C, as well as of the initial sample. Inhomogeneities in the form of carbide inclusions are evident in the surface structure, particularly distinguishable on samples treated for 3 and 5 min (Fig. 2c and 2d). Since AISI 304 steel lacks stabilizing alloying elements (Ti, Nb) that prevent the interaction of carbon with chromium, this material is prone to the precipitation of $Cr_{23}C_6$ carbides along grain boundaries during the production rolling stage as a result of heat treatment. This characteristic leads to a decrease in chromium content in the boundary regions, which in turn negatively affects corrosion resistance [29]. Because chromium carbide possesses significantly lower electrical conductivity compared to the metallic matrix [30], it dissolves to a lesser extent during EPT, resulting in the formation of characteristic relief along the grain boundaries. With increasing EPT duration, the number and size of carbide inclusions decrease. As a result of 10-min EPT, only isolated inclusions are observed in the structure.

During EPT of AISI 316L and AISI 321 steel samples, an increase in treatment duration leads only to the removal of microroughnesses and an overall reduction of the relief of the pre-ground surface. No significant changes in surface structure are observed. Micrographs of the sample surfaces after 5 min of EPT are presented in Fig. 3. Unlike AISI 304 steel, the AISI 316L steel surface shows no relief from carbide inclusions along grain boundaries (Fig. 3a). This is attributed, firstly, to its reduced carbon content (0.03 %). Secondly, the presence of molybdenum in AISI 316L steel impedes the diffusion of carbon and chromium atoms to grain boundaries, preventing carbide formation [31]. In AISI 321 steel, instead of undesirable chromium carbide inclusions, stable titanium carbide (TiC) inclusions form, which are distributed throughout the grain volume rather than being confined solely to the boundaries [32].

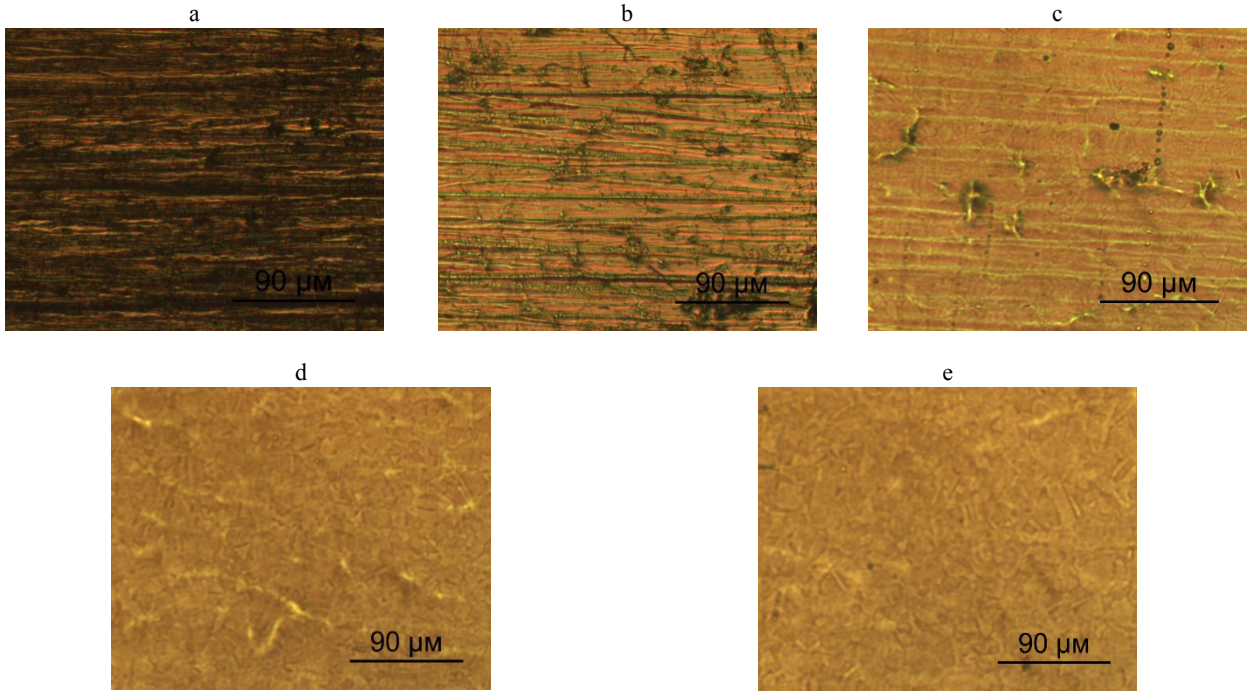

Fig. 2. Surface structure of AISI 304 steel samples before and after EPT with different durations:
a – initial sample; b – EPT 1 min; c – EPT 3 min; d – EPT 5 min; e – EPT 10 min

Consequently, after EPT, titanium carbide inclusions on AISI 321 steel samples appear as small uniformly dispersed particles with sizes not exceeding 4 μm (Fig. 3b). Furthermore, increasing the treatment duration up to 10 min does not cause any significant change in their quantity or size.

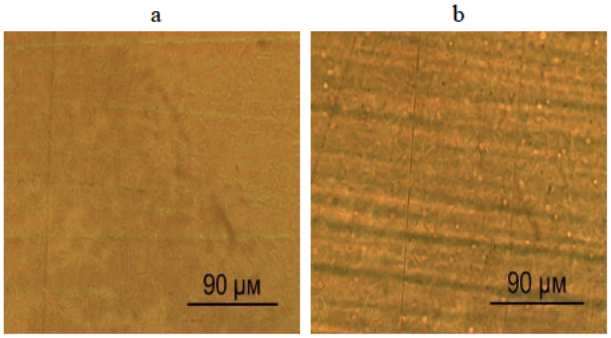

Fig. 3. Surface structure of AISI 316L (a) and AISI 321 (b) steel samples after EPT with a duration of 5 min

The identified features of the surface structure formation in AISI 304 steel have a significant impact on its roughness. In general, the dependencies characterizing the dynamics of roughness change (ΔRa) for all studied materials exhibit a similar trend (Fig. 4).

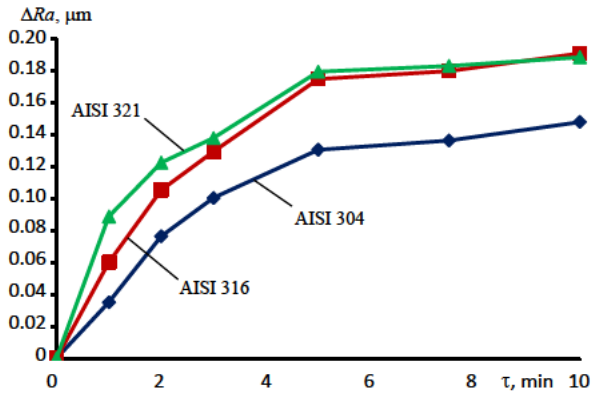

Fig. 4. Dynamics of surface roughness change for samples made of corrosion-resistant steels during EPT

The most intensive change in roughness is observed after EPT with a duration of 3–5 min, after which the rate of change noticeably decreases. However, due to the presence of relief formed by carbide inclusions, the ΔRa values for AISI 304 steel samples are significantly lower than for AISI 316L and AISI 321 steel samples. For instance, after 5 min of treatment, the change in roughness ΔRa for AISI 316L and AISI 321 steels is 0.17 μm and 0.18 μm, respectively, while for AISI 304 steel it is 0.13 μm (Fig. 4). Therefore, the presence of uniformly dispersed titanium carbide inclusions on the surface of AISI 321 steel samples does not have a significant effect on the roughness of the formed surface.

Fig. 5 presents the dependencies characterizing the influence of voltage on metal removal and surface roughness change, obtained for samples after EPT with a duration of 5 min and an electrolyte temperature of 90 °C. In the voltage range of 260–320 V, metal removal decreases according to a nearly linear dependence: from 1.79–1.90 % down to 1.37–1.41 %. Notably, metal removal for AISI 316 steel is significantly higher than for the other materials considered. When the voltage is increased to 340 V, a more intensive reduction in removal occurs – down to 1.12–1.19 % (Fig. 5a). This is associated with approaching the region where the process transitions into the electrolyte-discharge mode [25]. Despite the substantial influence of voltage on metal removal, the value of ΔRa in the range of 260–320 V remains practically unchanged and is: 0.124–0.131 μm for AISI 304 steel and 0.175–0.188 μm for AISI 316 and AISI 321 steels. However, at a voltage of 340 V, a significant deterioration in the quality of the formed surface is observed for all studied materials (Fig. 5b).

Table 2 presents the values of the change in roughness (ΔRa) and metal removal (Δm) for the studied materials resulting from EPT at different electrolyte temperatures (voltage 300 V). The presented data indicate that the higher the electrolyte temperature, the greater the polishing efficiency, defined as the change in roughness per unit mass of material removed from the treated surface ($\Delta Ra/\Delta m$). Depending on the material being treated, its value is: at a temperature of 70 °C – 0.05–0.07 μm/%, and at a temperature of 90 °C – 0.09–0.12 μm/% (Fig. 6).

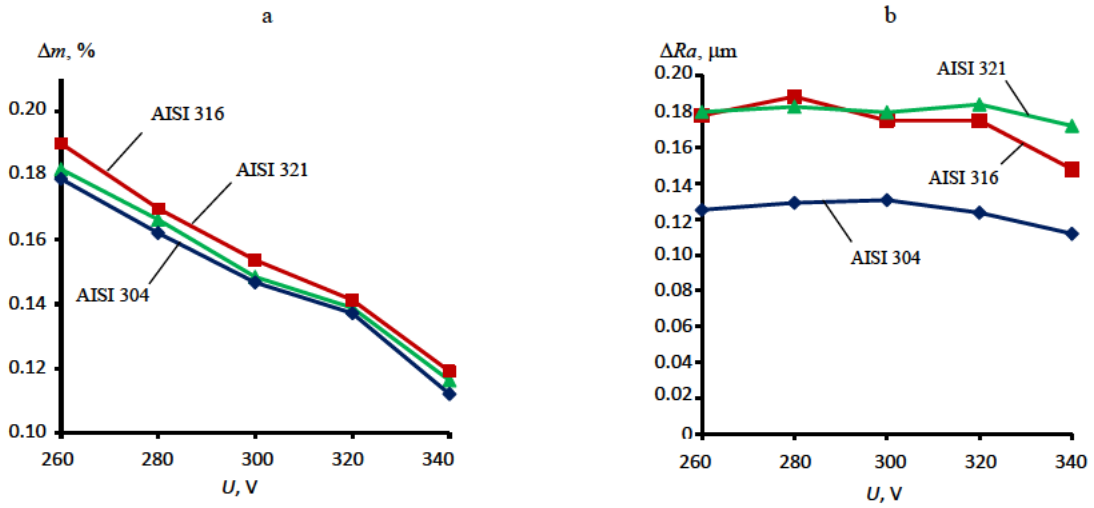

Fig. 5. Effect of EPT voltage on metal removal (a) and surface roughness change (b)

Table 2

Surface roughness and metal removal at various electrolyte temperature values

T, °C	Δ*Ra*, μm			Δ*m*, %		
	AISI 304	AISI 316	AISI 321	AISI 304	AISI 316	AISI 321
70	0.146	0.194	0.194	2.89	3.01	2.92
80	0.133	0.178	0.184	2.14	2.28	2.18
90	0.131	0.175	0.180	1.47	1.55	1.51

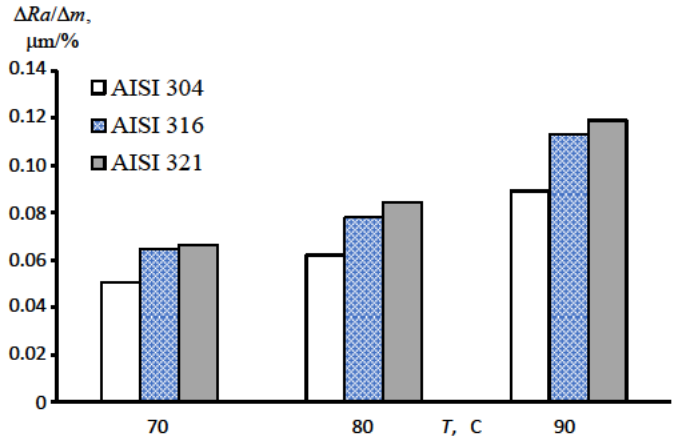

Fig. 6. Influence of electrolyte temperature on the efficiency of EPT (Δ*Ra*/Δ*m*)

The conducted potentiodynamic tests showed that EPT leads to an improvement in the protective properties of the formed surface for all investigated materials. To evaluate the influence of EPT duration on corrosion indicators, samples treated for 1, 3, 5, 7.5, and 10 min at a voltage of 300 V and an electrolyte temperature of 90 °C were used. As an example, Fig. 7 presents the polarization curves for AISI 316L steel samples, and Table 2 shows the values of corrosion potential E_{corr}, corrosion current density i_{corr}, and pitting potential E_{pitt} determined based on the obtained polarization curves. With an increase in EPT duration, the corrosion potential E_{corr} of the investigated materials, which determines thermodynamic stability, shifts towards more positive values. This indicates a transition of the treated surface into a passive state, characterized by a significant

reduction in anodic activity and, consequently, an increase in the material's corrosion resistance in the studied environment. The most noticeable shift is observed for AISI 316L steel samples – the corrosion potential increases from –184 mV in the initial state to –98 mV after 10 min of treatment. The least significant change in E_{corr} was noted for AISI 321 steel samples: from –230 mV in the initial state to –193 mV after 10 min of EPT.

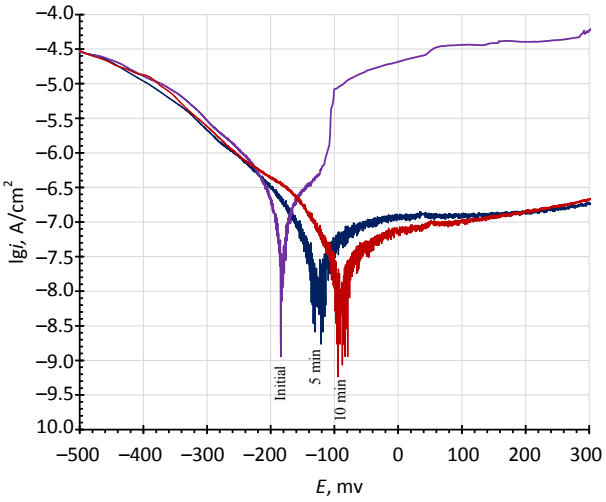

Fig. 7. Polarization curves of AISI 316L steel samples in E–lg$i$ coordinates

EPT has a significant influence on the corrosion current density, i_{corr}, which determines the rate of corrosion degradation. Its most intensive reduction occurs during the early stage of treatment (1 min). With a further increase in EPT duration, a more gradual decrease in i_{corr} is observed. After 10 min of treatment, the corrosion current density of the investigated materials decreases to i_{corr} = 0.041–0.066 μA/cm², which is 6.8–7.0 times lower compared to the initial values. As a result of EPT the pitting potential E_{pitt} increases. This parameter characterizes the threshold voltage value required for local breakdown of the protective passive film. Its value for all investigated stainless steels increases from 170–280 mV in the initial state to 660–710 mV after 10 min of treatment. The minimum values of corrosion current density and pitting potential are achieved for AISI 316L steel, while the maximum values are for AISI 304 steel.

When varying the electrolyte temperature in the range of 70–90 °C, despite a two-fold difference in metal removal, no significant change in corrosion resistance indicators was established. A certain improvement in corrosion resistance observed when decreasing the electrolyte temperature to 70 °C is explained in this case by a reduction in the height of microroughnesses on the treated surface. For example, for AISI 316L steel samples, decreasing the electrolyte temperature from 90 to 70 °C leads to a reduction in corrosion current density from 0.061 to 0.045 μA/cm² and an increase in pitting potential from 580 to 670 mV.

For all investigated materials, an increase in the EPT voltage to 340 V leads to a sharp decline in corrosion resistance indicators. For instance, compared to samples treated at 260–320 V, the corrosion current density increased by 1.6–2.5 times (Fig. 8). This behavior is attributed to approaching the transition region to the electrolytic discharge mode, in which the nature of the processes occurring in the vapor-gas envelope changes, as well as to a deterioration in the quality of the formed surface due to a lower metal removal rate. At the same time, no significant microstructural changes on the surface of the specimens treated at a voltage of 340 V were observed.

Table 3

Values of corrosion potential E_{corr}, corrosion current density i_{corr} and pitting potential E_{pitt} versus treatment duration τ

τ, min	E_{corr}, mV			i_{corr}, μA/cm²			E_{pitt}, mV		
	AISI 304	AISI 316	AISI 321	AISI 304	AISI 316	AISI 321	AISI 304	AISI 316	AISI 321
0 (initial)	–219	–184	–230	0.446	0.288	0.422	170	280	270
1	–207	–148	–190	0.129	0.134	0.123	205	430	355
3	–198	–124	–192	0.126	0.081	0.112	455	520	470
5	–177	–128	–189	0.087	0.061	0.093	520	580	515
7.5	–172	–114	–192	0.098	0.055	0.089	560	700	580
10	–147	–98	–193	0.066	0.041	0.060	680	710	660

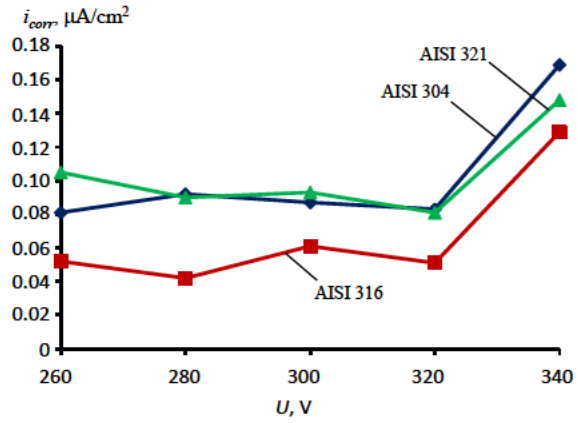

Fig. 8. Effect of EPT voltage on the corrosion current density of samples made of corrosion-resistant steels

The established improvement in the protective properties of the formed surface of the investigated materials resulting from EPT is a consequence of a complex change in its condition. EPT removes the defective surface layer with its increased dislocation density, which also contains microcracks, foreign inclusions, and tool wear products all of which serve as initiation sites for corrosion processes. The overall reduction in microroughness height during EPT also positively influences the surface's protective properties. Furthermore, EPT leads to the formation of a more uniform, continuous, and chemically stable passive oxide film on the surface, which possesses high resistance to the action of an aggressive environment containing chloride ions.

Since microrelief is a key factor determining wettability, it is evident that EPT, by smoothing it, will significantly affect the wetting contact angle of the studied stainless steels. Based on measurement results, it was established that the dependencies of the wetting contact angle on EPT duration for samples of all investigated materials are identical. During EPT with a duration of 1–3 mins, a sharp increase in the wetting contact angle is observed. For instance, after 3 min of treatment, its value increases from the initial state of 57.4–59.2° to 83.5–84.2°. After EPT with a duration of 5 min or more, the value of θ stabilizes within the range of 84.8–88.4°. It is important to note that the obtained wetting contact angle values were found to be similar for the different investigated materials. Thus, the identified structural inhomogeneities in the form of carbide inclusions, detected in the structure of AISI 304 and AISI 321 steels, do not have a significant influence on the magnitude of the wetting contact angle.

CONCLUSIONS

1. During EPT of AISI 304 steel, inhomogeneities in the form of chromium carbide inclusions appear in the surface structure; their size and quantity decrease with increasing treatment duration. On AISI 321 steel samples, titanium carbide inclusions manifest as small uniformly dispersed particles with sizes not exceeding 4 μm. The surface of AISI 316L steel samples shows no relief formed by carbide inclusions along grain boundaries.

2. The established features of surface structure formation in AISI 304 steel significantly influence its roughness. The most intensive change in roughness is observed after EPT lasting 3–5 min, after which the rate of change noticeably decreases. However, due to the presence of relief from carbide inclusions, the ΔRa values for AISI 304 steel samples are significantly lower than for AISI 316L and AISI 321 steel samples. After 5 min of treatment, the roughness change ΔRa for AISI 316L and AISI 321 steels is 0.17 μm and 0.18 μm, respectively, while for AISI 304 steel it is 0.13 μm. Thus, the presence of uniformly dispersed titanium carbide inclusions on the surface of AISI 321 steel samples does not significantly affect the roughness of the formed surface. Despite the substantial influence of voltage on material removal, the ΔRa value in the 260–320 V range remains practically unchanged: 0.124–0.131 μm for AISI 304 steel and 0.175–0.188 μm for AISI 316L and AISI 321 steels. However, at a voltage of 340 V, a significant deterioration in the quality of the formed surface is observed for all studied stainless steels, which is associated with approaching the transition region of the process into the electrolyte-discharge mode.

3. With increasing EPT duration, the corrosion potential (E_{corr}) of the studied stainless steels shifts towards more positive values. The most noticeable shift is observed for AISI 316L steel samples, where the corrosion potential increases from –184 mV in the initial state to –98 mV after 10 min

of treatment. The corrosion current density of the investigated materials decreases to i_{corr} = = 0.041–0.066 μA/cm², which is 6.8–7.0 times lower than the initial values. The pitting potential (E_{pitt}) increases from 170–280 mV in the initial state to 660–710 mV after 10 min of treatment.

4. It was established that the dependencies of the wetting contact angle on EPT duration for the studied materials are identical. After 3 min of treatment, its value increases from the initial range of 57.4–59.2° to 83.5–84.2°. Following EPT with a duration of 5 min or more, the wetting contact angle value stabilizes within the range of 84.8–88.4°.

REFERENCES

1. Sojitra P., Engineer Ch., Raval A., Kothwala D., Jariwala A., Kotadia H., Adeshara S., Mehta G. (2009) Surface Enhancement and Characterization of L-605 Cobalt Alloy Cardiovascular Stent by Novel Electrochemical Treatment. *Artificial Organs*, 23 (2), 55–64.
2. Rozhnova O. M., Pavlov V. V., Sadovoy M. A. (2015) Biological Compatibility of Metal-Based Medical Devices and Causes of Pathological Reactivity (Review). *Bulletin of Siberian Medicine*, 14 (4), 110–118. https://doi.org/10.20538/1682-0363-2015-4-110-118 (in Russian).
3. Zhang W., Li Z., Xu C., Chai M., Dong P. (2023) Surface Characteristics of NiTi Cardiovascular stents by Selective Laser Melting and Electrochemical Polishing. *International Journal of Advanced Manufacturing Technology*, 130 (1–2), 623–634. https://doi.org/10.1007/s00170-023-12734-x.
4. Burstein G., Vines S. (2001) Repetitive Nucleation of Corrosion Pits on Stainless Steel and the Effects of Surface Roughness. *Journal of The Electrochemical Society*, 148 (12), 504–516. https://doi.org/10.1149/1.1416503.
5. Lee S. M., Lee W. G., Kim Y. H., Jang H. (2012) Surface Roughness and Corrosion Resistance of 21Cr Ferritic Stainless Steel. *Corrosion Science*, 63, 404–409. https://doi.org/10.1016/j.corsci.2012.06.031.
6. Zelenina T. G., Fedchishin O. V., Trofimov V. V., Mansurova L. A., Smolyanko L. E. (2009) Investigation of biocompatible properties of implant materials. *Siberian Medical Journal (Irkutsk)*, 90 (7), 93–94 (in Russian).
7. Dibra A., Kastrati A., Mehilli J., Pache J., von Oepen R., Dirschinger J., Schömig A. (2005) Influence of Stent Surface Topography on Outcomes After Coronary Stenting. *Catheterization and Cardiovascular Interventions*, 65 (3), 374–380. https://doi.org/10.1002/ccd.20400.
8. De Scheerder I., Wang K., Sohier J., Verbeken E., Zhou X. R., Frooyen L., Van Humbeeck J., Van de Werf F. (1998) Metallic Surface Treatment by Electrochemical Polishing Reduces Thrombogenicity and Neointimal Hyperplasia After Stent Implantation. *Journal of the American College of Cardiology*, 31 (S1), 277. https://doi.org/10.1016/S0735-1097(98)81848-2.
9. Tepe G., Wendel H. P., Khorchidi S., Schmehl J., Wiskirchen J., Pusich B., Claussen C. D., Duda S. H. (2002) Thrombogenicity of Various Endovascular Stent Types: an in Vitro Evaluation. *Journal of Vascular and Interventional Radiology*, 13 (10), 1029–1035. https://doi.org/10.1016/s1051-0443(07)61868-5.
10. Bandyopadhyay A., Mitra I., Goodman S. B., Kumar M., Bose S. (2023) Improving Biocompatibility for Next Generation of Metallic Implants. *Progress in Materials Science*, 133, 101053. https://doi.org/10.1016/j.pmatsci.2022.101053.
11. Amirtharaj Mosas K. K., Chandrasekar A. R., Dasan A., Pakseresht A., Galusek D. (2022) Recent Advancements in Materials and Coatings for Biomedical Implants. *Gels*, 8 (5), 323. https://doi.org/10.3390/gels8050323.
12. Duan X., Yang Y., Zhang T., Zhu B., Wei G., Li H. (2024) Research Progress of Metal Biomaterials for Cardiovascular Stents and Surface Treatment Methods. *Heliyon*, 10 (4), e25515. https://doi.org/10.1016/j heliyon.2024. e25515.
13. Zaman H. A., Sharif S., Idris M. H., Kamarudin A. (2015) Metallic Biomaterials for Medical Implant Applications: a Review. *Applied Mechanics and Materials*, 735, 19–25. https://doi.org/10.4028/www.scientific net/AMM.735.19.
14. Korolyov A., Bubulis A., Vėžys J., et al. (2021). Electrolytic Plasma Polishing of NiTi Alloy. *Mathematical Models in Engineering*, 7 (4), 70–80. https://doi.org/10.21595/mme.2021.22351.
15. Lisovskaya Yu. O., Alekseev Yu. G., Korolyov A. Yu., Niss V. S., Fomikhina I. V. (1998) Study of the Structure, Surface Morphology, Roughness Parameters and Corrosion Resistance of the Surface Layer of Stainless Steel During Electrolytic-Plasma Treatment. Svarka i rodstvennye tekhnologii: Resp. mezhvedomstv. sb. nauch. tr [Welding and related technologies: Republican interdepartmental collection of scientific papers]. Minsk, Iss. 9, 63–69 (in Russian).
16. Ji G., Ma L., Zhang S., Zhang J., Wu L. (2025) Study of Electrochemical Behavior and a Material Removal Mechanism During Electrolytic Plasma Polishing of 316L Stainless Steel. Materials, 18 (6), 1307. https://doi.org/10.3390/ma18061307
17. Zatkalíková V., Podhorský Š., Štrbák M., Liptáková T., Markovičová L., Kuchariková L. (2022) Plasma Electrolytic Polishing—An Ecological Way for Increased Corrosion Resistance in Austenitic Stainless Steels. Materials, 15 (12), 4223. https://doi.org/10.3390/ma15124223
18. Korolyov A. Yu., Tomilo V. A. (2024). Electrolytic Plasma Polishing of Metallic Materials for Medical Purposes. *Aktual'nye problemy prochnosti: materialy LXVIII mezhdunarodnoi nauchnoi konferentsii: Vitebsk, 27–31 maya 2024 g.* [Current Strength Issues: Proceedings of the LXVIII International Scientific Conference: Vitebsk, May 27-31, 2024]. Minsk, 2024, 328–330 (in Russian).
19. Zeidler H., Boettger-Hiller F., Edelmann J., Schubert A. (2016) Surface Machining of Medical Parts Using Plasma Electrolytic Polishing. *Procedia CIRP*, 49, 83–87. https://doi.org/10.1016/j.procir.2015.07.038.

20. Kulikov I. S., Vashchenko S. V., Kamenev A. Ya. (2010) *Electrolytic-Plasma Processing of Materials*. Minsk, Belaruskaya Navuka Publ. 232 (in Russian).
21. Smyslov A. M., Smyslova M. K., Mingazhev A. Dz., Selivanov K. S. (2009) Multistage Elektrolitplasma Processing of Products From the Titan and Titanic Alloys. *Vestnik USATU*, 13 (1), 141–145 (in Russian).
22. Navickaitė K., Ianniciello L., Tušek J., Engelbrecht K., Bahl C. R. H., Penzel M., Nestler K., Böttger-Hiller F., Zeidler H. (2021) Plasma Electrolytic Polishing of Nitinol: Functional Properties. *Materials*, 14 (21), 6450. https://doi.org/10.3390/ma14216450.
23. Alekseev Yu. G., Korolyov A. Yu., Niss V. S. (2019) Electrolytic-Plasma Polishing of Biomedical Co–Cr alloys. *Vestsi Natsyyanal'nai akademii navuk Belarusi. Seryya fizika-technichnych navuk = Proceedings of the National Academy of Sciences of Belarus. Physical-technical series*, 64 (3), 296–303. https://doi.org/10.29235/1561-8358-2019-64-3-296-303 (in Russian).
24. Aliakseyeu Y., Bubulis A., Minchenya V., Korolyov A., Niss V., Kandrotaitė Janutienė R. (2021) Plasma Electrolyte Polishing of Ti and Nb Alloys. *Mechanika*, 27 (1), 88–93. https://doi.org/10.5755/j02 mech.25044.
25. Sinkevich Yu. V., Sheleg V. K., Yankovsky I. N., Belyaev G. Ya. (2014) *Electropulse Polishing of Fe-Cr-Ni Alloys*. Minsk, BNTU. 325 (in Russian).
26. Dhaiveegan P., Elangovan N., Nishimura T., Rajendran N. (2016) Corrosion Behavior of 316L and 304 Steels in Multiple Environments. *RSC Advances*, 6 (53), 47314–47324. https://doi.org/10.1039/C6RA04015B.
27. Osipovich K., Kalashnikov K., Vorontsov A. (2019) Alloying Effect of Ti-6Al-4V on 321 Steel Processed by EBAM. *IOP Conference Series: Materials Science and Engineering*, 537 (2), 022075. https://doi.org/10.1088/1757-899X/537/2/022075.
28. Rybalko K. V., Beketayeva L. A., Davydov A. D. (2014) Estimation of corrosion Current by the Analysis of Polarization Curves: Electrochemical Kinetics Mode. *Russian Journal of Electrochemistry*, 50 (2), 108–113. https://doi.org/10.1134/s1023193514020025.
29. Rashid M. W. A., Gakim M., Rosli Z. M., Azam M. A. (2012) Formation of Cr23C6 during sensitization of AISI 304 steel. *International Journal of Electrochemical Science,* 7 (10), 9465–9477. https://doi.org/10.1016/s1452-3981(23)16211-0.
30. White G. K., Woods S. B. (eds.). (1982) *Landolt-Börnstein: Metals – Electronic Transport Phenomen*a. New York, Springer. 337 p.
31. Padilha A. F., Rios P. R. (2002) Decomposition of Austenite in Stainless Steels. *ISIJ International*, 42 (4), 325–337. https://doi.org/10.2355/isijinternational.42.325.
32. Cramer S. D., Covino B. S. (eds.). (2003) *Corrosion: Fundamentals, Testing, and Protection. ASM Handbook. Vol. 13A*. ASM International. 1118 https://doi.org/10.31399/asm hb.v13a.9781627081825.

Received: 25.10.2025
Accepted: 29.12.2025
Published online: 30.01.2026